

1

2 **Molecular mechanism for antibody-dependent enhancement of coronavirus entry**

3

4 Yushun Wan ^{1,*}, Jian Shang ^{1,*}, Shihui Sun, Wanbo Tai ³, Jing Chen ⁴, Qibin Geng ¹,
5 Lei He ², Yuehong Chen ², Jianming Wu ¹, Zhengli Shi ⁴, Yusen Zhou, Lanying Du ^{3,#},
6 Fang Li ^{1,#}

7

8 ¹ Department of Veterinary and Biomedical Sciences, College of Veterinary Medicine,
9 University of Minnesota, Saint Paul, MN, USA

10 ² Laboratory of infection and immunity, Beijing Institute of Microbiology and
11 Epidemiology, Beijing, China

12 ³ Lindsley F. Kimball Research Institute, New York Blood Center, New York, NY, USA

13 ⁴ Wuhan Institute of Virology, Chinese Academy of Sciences, Wuhan, Hubei Province,
14 China

15

16 * These authors contributed equally to this work. Author order was determined by the
17 time to join the project.

18

19 # Correspondence:

20

21 Fang Li (lifang@umn.edu); Lanying Du (LDu@nybc.org)

22

23

24 Keywords: antibody-dependent enhancement of viral entry, MERS coronavirus, SARS
25 coronavirus, spike protein, neutralizing antibody, viral receptor, IgG Fc receptor

26

27 Running title: Coronavirus entry mediated by neutralizing antibodies

28

29 **Abstract**

30 Antibody-dependent enhancement (ADE) of viral entry has been a major concern
31 for epidemiology, vaccine development and antibody-based drug therapy. However, the
32 molecular mechanism behind ADE is still elusive. Coronavirus spike protein mediates
33 viral entry into cells by first binding to a receptor on host cell surface and then fusing
34 viral and host membranes. Here we investigated how a neutralizing monoclonal antibody
35 (mAb), which targets the receptor-binding domain (RBD) of MERS coronavirus spike,
36 mediates viral entry using pseudovirus entry and biochemical assays. Our results showed
37 that mAb binds to the virus-surface spike, allowing it to undergo conformational changes
38 and become prone to proteolytic activation. Meanwhile, mAb binds to cell-surface IgG
39 Fc receptor, guiding viral entry through canonical viral-receptor-dependent pathways.
40 Our data suggest that the antibody/Fc-receptor complex functionally mimics viral
41 receptor in mediating viral entry. Moreover, we characterized mAb dosages in viral-
42 receptor-dependent, antibody-dependent, and both-receptors-dependent entry pathways,
43 delineating guidelines on mAb usages in treating viral infections. Our study reveals a
44 novel molecular mechanism for antibody-enhanced viral entry and can guide future
45 vaccination and antiviral strategies.

46

47

48

49 **Significance**

50 Antibody-dependent enhancement (ADE) of viral entry has been observed for
51 many viruses. It was shown that antibodies target one serotype of viruses but only sub-
52 neutralize another, leading to ADE of the latter viruses. Here we identify a novel
53 mechanism for ADE: a neutralizing antibody binds to the virus-surface spike protein of
54 coronaviruses like a viral receptor, triggers a conformational change of the spike, and
55 mediates viral entry into IgG-Fc-receptor-expressing cells through canonical viral-
56 receptor-dependent pathways. We further evaluated how antibody dosages impacted viral
57 entry into cells expressing viral receptor, Fc receptor, or both receptors. This study
58 reveals complex roles of antibodies in viral entry and can guide future vaccine design and
59 antibody-based drug therapy.

60

61

62 **Introduction**

63 Antibody-dependent enhancement (ADE) occurs when antibodies facilitate viral
64 entry into host cells and enhance viral infection in these cells (1, 2). ADE has been
65 observed for a variety of viruses, most notably in flaviviruses (e.g., dengue virus) (3-6). It
66 has been shown that when patients are infected by one serotype of dengue virus (i.e.,
67 primary infection), they produce neutralizing antibodies targeting the same serotype of
68 the virus. However, if they are later infected by another serotype of dengue virus (i.e.,
69 secondary infection), the preexisting antibodies cannot fully neutralize the virus. Instead,
70 the antibodies first bind to the virus, then bind to the IgG Fc receptors on immune cells,
71 and mediate viral entry into these cells. Similar mechanism has been observed for HIV
72 and Ebola virus (7-10). Thus, sub-neutralizing antibodies (or non-neutralizing antibodies
73 in some cases) are responsible for ADE of these viruses. Given the critical roles of
74 antibodies in host immunity, ADE causes serious concerns in epidemiology, vaccine
75 design and antibody-based drug therapy. This study reveals a novel mechanism for ADE
76 where fully neutralizing antibodies mimic the function of viral receptor in mediating viral
77 entry into Fc-receptor-expressing cells.

78 Coronaviruses are a family of large, positive-stranded, and enveloped RNA
79 viruses (11, 12). Two highly pathogenic coronaviruses, SARS coronavirus (SARS-CoV)
80 and MERS coronavirus (MERS-CoV), cause lethal infections in humans (13-16). An
81 envelope-anchored spike protein guides coronavirus entry into host cells (17). As a
82 homo-trimer, the spike contains three receptor-binding S1 subunits and a trimeric
83 membrane-fusion S2 stalk (18-25). This state of the spike on the mature virions is called
84 “pre-fusion”. SARS-CoV and MERS-CoV recognize angiotensin-converting enzyme 2

85 (ACE2) and dipeptidyl peptidase 4 (DPP4), respectively, as their viral receptor (26-28).
86 Their S1 each contains a receptor-binding domain (RBD) that mediates receptor
87 recognition (29, 30) (Fig. 1A). The RBD is located on the tip of the spike trimer and is
88 present in two different states – standing up and lying down (18, 21) (Fig. 1B). Binding
89 to a viral receptor can stabilize the RBD in the standing-up state (20). Receptor binding
90 also triggers the spike to undergo further conformational changes, allowing host proteases
91 to cleave at two sites sequentially – first at the S1/S2 boundary (i.e., S1/S2 site) and then
92 within S2 (i.e., S2' site) (31, 32). Proteolysis of the spike can take place during viral
93 maturation (by proprotein convertases), after viral release (by extracellular proteases),
94 after viral attachment (by cell-surface proteases), or after viral endocytosis (by lysosomal
95 proteases) (33-39). After two protease cleavages, S1 dissociates and S2 undergoes a
96 dramatic structural change to fuse host and viral membranes; this membrane-fusion state
97 of the spike is called “post-fusion” (40, 41). Due to the recent progresses towards
98 understanding the receptor recognition and membrane fusion mechanisms of coronavirus
99 spikes, coronaviruses represent an excellent model system for investigating ADE of viral
100 entry.

101 ADE has been observed for coronaviruses. Several studies have shown that sera
102 induced by SARS-CoV spike enhance viral entry into Fc-receptor-expressing cells (42-
103 44). Further, one study demonstrated that unlike receptor-dependent viral entry, sera-
104 dependent SARS-CoV entry does not go through the endosome pathway (44).
105 Additionally, it has long been known that immunization of cats with feline coronavirus
106 spike leads to worsened future infection due to the induction of infection-enhancing
107 antibodies (45-47). However, detailed molecular mechanisms for ADE of coronavirus

108 entry are still unknown. We previously discovered a monoclonal antibody (mAb) (named
109 Mersmab1), which has strong binding affinity for MERS-CoV RBD and efficiently
110 neutralizes MERS-CoV entry by outcompeting DPP4 (48); this discovery allowed us to
111 comparatively study the molecular mechanisms for antibody-dependent and receptor-
112 dependent viral entries.

113 In this study, we examined how Mersmab1 binds to MERS-CoV spike, triggers
114 the spike to undergo conformational changes, and mediates viral entry into Fc-receptor-
115 expressing cells. We also investigated the pathways and antibody dosages for Mersmab1-
116 dependent and DPP4-dependent viral entries. Our study sheds lights on the mechanisms
117 of ADE and provides insight into vaccine design and antibody-based antiviral drug
118 therapy.

119

120 **Results**

121 **Antibody-dependent enhancement of coronavirus entry**

122 To investigate ADE of coronavirus entry, we first characterized the interactions
123 between Mersmab1 (which is a MERS-CoV-RBD-specific mAb) and MERS-CoV spike
124 using biochemical methods. First, ELISA was performed between Mersmab1 and MERS-
125 CoV RBD and between Mersmab1 and MERS-CoV spike ectodomain (S-e) (Fig. 2A). To
126 this end, Mersmab1 (which was in excess) was coated to the ELISA plate, and gradient
127 amounts of recombinant RBD or S-e were added for detection of potential binding to
128 Mersmab1. The result showed that both the RBD and S-e bound to Mersmab1. S-e bound
129 to Mersmab1 more tightly than the RBD did, likely due to the multivalent effects

130 associated with the trimeric state of S-e. Second, we prepared Fab from Mersmab1 using
131 papain digestion and examined the binding between Fab and S-e using ELISA. Here
132 recombinant S-e (which was in excess) was coated to the ELISA plate, and gradient
133 amounts of Fab or Mersmab1 were added for detection of potential binding to S-e. The
134 result showed that both Fab and Mersmab1 bound to S-e (Fig. 2B). Mersmab1 bound to
135 S-e more tightly than Fab did, also likely due to the multivalent effects associated with
136 the dimeric state of Mersmab1. Third, flow cytometry assay was carried out to detect the
137 binding between S-e and DPP4 receptor and among S-e, Mersmab1 and CD32A (which
138 is an Fc receptor). To this end, DPP4 or CD32A was expressed on the surface of human
139 HEK293T cells (human kidney cells), and recombinant S-e was added for detection of
140 potential binding to one of the two receptors in the absence or presence of Mersmab1.
141 The result showed that without Mersmab1, S-e bound to DPP4 only; in the presence of
142 Mersmab1, S-e bound to CD32A (Fig. 2C). As a negative control, a SARS-CoV RBD-
143 specific mAb (49) did not mediate the binding of S-e to CD32A. The cell-surface
144 expressions of both DPP4 and CD32A were measured and used for calibrating the flow
145 cytometry result (Fig. 2D), demonstrating that the direct binding of S-e to DPP4 is
146 stronger than the indirect binding of S-e to CD32A through Mersmab1. Overall, these
147 biochemical results reveal that Mersmab1 not only directly binds to the RBD region of
148 MERS-CoV S-e, but also mediates the indirect binding interactions between MERS-CoV
149 S-e and the Fc receptor.

150 Next we investigated whether Mersmab1 mediates MERS-CoV entry into Fc-
151 receptor-expressing cells. To this end, we performed MERS-CoV pseudovirus entry
152 assay, where retroviruses pseudotyped with MERS-CoV spike (i.e., MERS-CoV

153 pseudoviruses) were used to enter human cells expressing CD32A on their surface. The
154 main advantage of pseudovirus entry assay is to focus on the viral entry step (which is
155 mediated by MERS-CoV spike) by separating viral entry from the other steps of viral
156 infection cycles (e.g., replication, packaging and release). We tested three different types
157 of Fc receptors: CD16A, CD32A, and CD64A; each of these Fc receptors was
158 exogenously expressed in HEK293T cells. We also tested macrophage cells where
159 mixtures of Fc receptors were endogenously expressed. Absence of Mersmab1 served as
160 a control for Mersmab1 (a non-neutralizing mAb would be appropriate as another control
161 for Mersmab1, but we do not have access to any non-neutralizing mAb). The result
162 showed that in the absence of Mersmab1, MERS-CoV pseudoviruses could not enter Fc-
163 receptor-expressing cells; in the presence of Mersmab1, MERS-CoV pseudoviruses
164 demonstrated significant efficiency in entering CD32A-expressing HEK293T cells and
165 macrophage cells (Fig. 3A). In comparison, in the absence of Mersmab1, MERS-CoV
166 pseudoviruses entered DPP4-expressing HEK293T cells efficiently, but the entry was
167 blocked effectively by Mersmab1 (Fig. 3A). In control experiments, anti-SARS mAb did
168 not mediate MERS-CoV pseudoviruses entry into Fc-receptor-expressing HEK293T cells
169 or macrophages, and neither did it block MERS-CoV pseudoviruses entry into DPP4-
170 receptor-expressing HEK293T cells (Fig. 3A). In another set of control experiments, we
171 showed that neither the Fc nor the Fab portion of Mersmab1 could mediate MERS-CoV
172 pseudoviruses entry into Fc-receptor-expressing HEK293T cells or macrophages (Fig.
173 3B), suggesting that both the Fc and Fab portions of anti-MERS mAb are required for
174 antibody-mediated viral entry. Here the above DPP4-expressing HEK293T cells were
175 induced to exogenously express high levels of DPP4. To detect background expression

176 levels of DPP4, we performed qRT-PCR on HEK293T cells. The result showed that
177 HEK293T cells express very low levels of DPP4 (Fig. 3C). In comparison, MRC5 cells
178 (human lung cells) express high levels of DPP4, whereas Hela cells (human cervical
179 cells) do not express DPP4 (Fig. 3C). Because of the comprehensive control experiments
180 that we performed, the very low endogenous expression of DPP4 in HEK293T cells
181 should not affect our conclusions. Nevertheless, we confirmed the above results using
182 Hela cells that do not express DPP4 (Fig. 3D). Overall, our results reveal that Mersmab1
183 mediates MERS-CoV entry into Fc-receptor-expressing cells, but blocks MERS-CoV
184 entry into DPP4-expressing cells.

185 To expand the above observations to another coronavirus, we investigated ADE
186 of SARS-CoV entry. We previously identified a SARS-CoV-RBD-specific mAb, named
187 33G4, which binds to the ACE2-binding region of SARS-CoV RBD (49, 50); this mAb
188 was examined here for its potential capability to mediate ADE of SARS-CoV entry (Fig.
189 3E). The result showed that 33G4 mediated SARS-CoV pseudovirus entry into CD32A-
190 expressing cells, but blocked SARS-CoV pseudovirus entry into ACE2-expressing cells.
191 Therefore, both the MERS-CoV-RBD-specific mAb and the SARS-CoV-RBD specific
192 mAb can mediate the respective coronavirus to enter Fc-receptor-expressing human cells,
193 while blocking the entry of the respective coronavirus into viral-receptor-expressing
194 human cells. For the remaining of this study, we selected the MERS-CoV-RBD-specific
195 mAb, Mersmab1, for in-depth analysis of ADE.

196 **Molecular mechanism for antibody-dependent enhancement of coronavirus entry**

197 To understand the molecular mechanism of ADE, we investigated whether
198 Mersmab1 triggers any conformational change of MERS-CoV spike. It was shown
199 previously that DPP4 binds to MERS-CoV spike and stabilizes the RBD in the standing-
200 up position (Fig. 1A, 1B), resulting in a weakened spike structure and allowing the S2'
201 site to become exposed to proteases (51). Here we repeated this experiment: MERS-CoV
202 pseudoviruses were incubated with DPP4 and then subjected to trypsin cleavage (Fig.
203 4A). The result showed that during the viral packaging process, virus-surface-anchored
204 MERS-CoV spike molecules were cleaved at the S1/S2 site by proprotein convertases; in
205 the absence of DPP4, the spike molecules could not be cleaved further at the S2' site by
206 trypsin. These data suggest that only the S1/S2 site, but not the S2' site, was accessible to
207 proteases in the free form of the spike trimer. In the presence of DPP4, a significant
208 amount of MERS-CoV spike molecules were cleaved at the S2' site by trypsin, indicating
209 that DPP4 binding triggered a conformational change of MERS-CoV spike to expose the
210 S2' site. Interestingly, we found that Mersmab1 binding also allowed MERS-CoV spike
211 to be cleaved at the S2' site by trypsin. As a negative control, the SARS-CoV-RBD-
212 specific mAb did not trigger MERS-CoV spike to be cleaved at the S2' site by trypsin.
213 Hence, like DPP4, Mersmab1 triggers a similar conformational change of MERS-CoV
214 spike to expose the S2' site for proteolysis.

215 We further analyzed the binding between Mersmab1 and MERS-CoV S-e using
216 negative-stain electron microscopy (EM). We previously demonstrated through
217 mutagenesis studies that Mersmab1 binds to the same receptor-binding region on MERS-
218 CoV RBD as DPP4 does (Fig. 1C) (48). Because full-length Mersmab1 (which is a
219 dimer) triggered aggregation of S-e (which is a trimer), we prepared the Fab part (which

220 is a monomer) of Mersmab1, detected the binding between Fab and S-e (Fig. 2B), and
221 used Fab in the negative-stain EM study. The result showed that Fab bound to the tip of
222 the S-e trimer, where the RBD is located (Fig. 4B). Due to the limited resolution of
223 negative-stain EM, we could not clearly see the conformation of the Fab-bound RBD.
224 However, based on previous studies, the receptor-binding site on the RBD in the spike
225 trimer is only accessible when the RBD is in the standing-up position (18, 20, 21). Hence,
226 the fact that the mAb binds to the receptor-binding region of the RBD in the spike trimer
227 suggests that the RBD is in the standing-up state. Thus, the results from negative-stain
228 EM and the proteolysis study are consistent with each other, supporting that like DPP4,
229 Mersmab1 stabilizes the RBD in the standing-up position and triggers a conformational
230 change of the spike. Future study on the high-resolution cryo-EM structure of MERS-
231 CoV S-e trimer complexed with Mersmab1 will be needed to provide detailed structural
232 information for the Mersmab1-triggered conformational changes of MERS-CoV S-e.

233 To understand the pathways of Mersmab1-dependent MERS-CoV entry, we
234 evaluated the potential impact of different proteases on MERS-CoV pseudovirus entry;
235 these proteases are distributed along the viral entry pathway. First, proprotein convertase
236 inhibitor (PPCi) was used for examining the role of proprotein convertases in the
237 maturation of MERS-CoV spike and the impact of proprotein convertases on the ensuing
238 Mersmab1-dependent viral entry (Fig. 5A). The result showed that when MERS-CoV
239 pseudoviruses were produced from HEK293T cells in the presence of PPCi, the cleavage
240 of MERS-CoV spike by proprotein convertases was significantly inhibited (Fig. 5B). In
241 the absence of Mersmab1, MERS-CoV pseudoviruses packaged in the presence of PPCi
242 entered DPP4-expressing human cells more efficiently than those packaged in the

243 absence of PPCi (Fig. 5A). In the presence of Mersmab1, MERS-CoV pseudoviruses
244 packaged in the presence of PPCi entered CD32A-expressing cells more efficiently than
245 those packaged in the absence of PPCi (Fig. 5A). These data suggest that proprotein
246 convertases play a role (albeit not as drastic as some other proteases; see below) in both
247 DPP4-dependent and Mersmab1-dependent MERS-CoV entry. Second, cell-surface
248 protease TMPRSS2 (transmembrane Serine Protease 2) was introduced to human cells
249 for evaluation of its role in Mersmab1-dependent viral entry (Fig. 5C). The result showed
250 that in the absence of Mersmab1, TMPRSS2 enhanced MERS-CoV pseudovirus entry
251 into DPP4-expressing cells, consistent with previous reports (36). In the presence of
252 Mersmab1, TMPRSS2 also enhanced MERS-CoV pseudovirus entry into CD32A-
253 expressing cells, suggesting that TMPRSS2 activates Mersmab1-dependent MERS-CoV
254 entry. Third, lysosomal protease inhibitors were evaluated for the role of lysosomal
255 proteases in Mersmab1-dependent viral entry (Fig. 5D). Two inhibitors were used,
256 lysosomal acidification inhibitor Baf-A1 and cysteine protease inhibitor E64d. The result
257 showed that lysosomal protease inhibitors blocked the DPP4-dependent viral entry
258 pathway, consistent with previous reports (39). Lysosomal protease inhibitors also
259 blocked the Mersmab1-dependent viral entry pathway, suggesting that lysosomal
260 proteases play important roles in Mersmab1-dependent MERS-CoV entry. Taken
261 together, the DPP4-dependent and Mersmab1-dependent MERS-CoV entries can both be
262 activated by proprotein convertases, cell-surface proteases, and lysosomal proteases;
263 hence the same pathways are shared by DPP4-dependent and Mersmab1-dependent
264 MERS-CoV entries.

265 **Antibody dosages for antibody-dependent enhancement of coronavirus entry**

266 To determine the range of Mersmab1 dosages in ADE, MERS-CoV pseudovirus
267 entry was performed in the presence of different concentrations of Mersmab1. Three
268 types of human HEK293T cells were used: HEK293T cells exogenously expressing
269 DPP4 only, CD32A only, or both DPP4 and CD32A. Accordingly, three different results
270 were obtained. First, as the amount of Mersmab1 increased, viral entry into DPP4-
271 expressing HEK293T cells continuously dropped (Fig. 6A). This result reveals that
272 Mersmab1 blocks the DPP4-dependent viral entry pathway by outcompeting DPP4 for
273 binding to MERS-CoV spike. Second, as the amount of Mersmab1 increased, viral entry
274 into CD32A-expressing HEK293T cells first increased and then decreased (Fig. 6A). The
275 turning point was about 100 ng/ml Mersmab1. A likely explanation for this result is as
276 follows: at low concentrations, more mAb molecules enhance the indirect interactions
277 between MERS-CoV spike and the Fc receptor; at high concentrations, mAb molecules
278 saturate the cell-surface Fc receptor molecules and then further bind to MERS-CoV spike
279 and block the indirect interactions between MERS-CoV spike and the Fc receptor. Third,
280 as the amount of Mersmab1 increased, viral entry into cells expressing both DPP4 and
281 CD32A first dropped, then increased, and finally dropped again (Fig. 6B). This result is
282 the cumulous effect of the previous two results. It reveals that when both DPP4 and
283 CD32A are present on host cell surface, Mersmab1 inhibits viral entry (by blocking the
284 DPP4-dependent entry pathway) at low concentrations, promotes viral entry (by
285 enhancing the CD32A-dependent entry pathway) at intermediate concentrations, and
286 inhibits viral entry (by blocking both the DPP4- and CD32A-dependent entry pathways)
287 at high concentrations. We further confirmed the above results using MRC5 cells, which
288 are human lung cells endogenously expressing DPP4 (Fig. 6C, 6D). Therefore, ADE of

289 MERS-CoV entry depends on the range of Mersmab1 dosages as well as expressions of
290 the viral and Fc receptors on cell surfaces.

291 **Discussions**

292 ADE of viral entry has been observed and studied extensively in flaviviruses,
293 particularly dengue virus (3-6). It has also been observed in HIV and Ebola viruses (7-
294 10). For these viruses, it has been proposed that primary viral infections of hosts led to
295 production of antibodies that are sub-neutralizing or non-neutralizing for secondary viral
296 infections; these antibodies cannot completely neutralize secondary viral infections, but
297 instead guide virus particles to enter Fc-receptor-expressing cells. ADE can lead to
298 worsened symptoms in secondary viral infections, causing major concerns for
299 epidemiology. ADE is also a major concern for vaccine design and antibody-based drugs
300 therapy, since antibodies generated or used in these procedures may lead to ADE. ADE
301 has been observed in coronavirus for decades, but the molecular mechanisms are
302 unknown. Recent advances in understanding the receptor recognition and cell entry
303 mechanisms of coronaviruses have allowed us to use coronaviruses as a model system for
304 studying ADE.

305 In this study we first demonstrated that a MERS-CoV-RBD-specific neutralizing
306 mAb binds to the RBD region of MERS-CoV spike and further showed that the mAb
307 mediates MERS-CoV pseudovirus entry into Fc-receptor-expressing human cells.
308 Moreover, a SARS-CoV-RBD-specific neutralizing mAb mediates ADE of SARS-CoV
309 pseudovirus entry. These results demonstrated that ADE of coronaviruses is mediated by
310 neutralizing mAbs that target the RBD of coronavirus spikes. In addition, the same

311 coronavirus strains that led to the production of fully neutralizing mAbs can be mediated
312 to go through ADE by these neutralizing mAbs. Our results differ from previously
313 observed ADE of flaviviruses where primary infections and secondary infections are
314 caused by two different viral strains and where ADE-mediating mAbs are only sub-
315 neutralizing or non-neutralizing for secondary viral infections (3-6). Therefore, our study
316 expands the concept of ADE of viral entry.

317 We then examined the molecular mechanism for ADE of coronavirus entry. We
318 showed that the mAb binds to the tip of MERS-CoV spike trimer, where the RBD is
319 located. mAb binding likely stabilizes the RBD in the standing-up position, triggers a
320 conformational change of MERS-CoV spike, and exposes the previously inaccessible S2'
321 site to proteases. During the preparation of this manuscript, a newly published study
322 demonstrated that a SARS-CoV-RBD-specific mAb (named S230) bound to the ACE2-
323 binding region in SARS-CoV RBD, stabilized the RBD in the standing-up position, and
324 triggered conformational changes of SARS-CoV spike (Fig. 7A) (52). In contrast, a
325 MERS-CoV-RBD-specific mAb (named LCA60) bound to the side of MERS-CoV RBD,
326 away from the DPP4-binding region, stabilized the RBD in the lying-down position, and
327 did not trigger conformational changes of MERS-CoV spike (Fig. 7B). These published
328 results are consistent with our result on Mersmab1-triggered conformational changes of
329 MERS-CoV spike, together suggesting that in order to trigger conformational changes of
330 coronavirus spikes, mAbs need to bind to the receptor-binding region in their RBD and
331 stabilize the RBD in the standing-up position. Moreover, our study revealed that ADE of
332 MERS-CoV entry follows the same entry pathways of DPP4-dependent MERS-CoV
333 entry. Specifically, proprotein convertases partially activate MERS-CoV spike. If cell-

334 surface proteases are present, MERS-CoV spike can be further activated and fuse
335 membranes on the cell surface; otherwise, MERS-CoV enters endosomes and lysosomes,
336 where lysosomal proteases activate MERS-CoV spike for membrane fusion. Taken
337 together, RBD-specific neutralizing mAbs bind to the same region on coronavirus spikes
338 as viral receptors do, trigger conformational changes of the spikes as viral receptors do,
339 and mediate ADE through the same pathways as viral-receptor-dependent viral entries. In
340 other words, RBD-specific neutralizing mAbs mediate ADE of coronavirus entry by
341 functionally mimicking viral receptors.

342 Finally we analyzed ADE of coronavirus entry at different antibody dosages.
343 MERS-CoV entry into cells expressing both viral and Fc receptors demonstrates complex
344 mAb-dosage-dependent patterns. As the concentration of mAb increases, (i) viral entry
345 into DPP4-expressing cells is inhibited more efficiently because mAb binds to the spike
346 and blocks the DPP4-dependent entry pathway, (ii) viral entry into Fc-receptor-
347 expressing cells is first enhanced and then inhibited because mAb binds to the Fc receptor
348 to enhance the ADE pathway until the Fc receptor molecules are saturated, and (iii) viral
349 entry into cells expressing both DPP4 and Fc receptor is first inhibited, then enhanced,
350 and finally inhibited again because of the cumulative effects of the previous two patterns.
351 In other words, for viral entry into cells expressing both DPP4 and Fc receptor, there
352 exist a balance between the DPP4-dependent and antibody-dependent entry pathways that
353 can be shifted and determined by mAb dosages. Importantly, ADE occurs only at
354 intermediate mAb dosages. Our study explains an earlier observation where ADE of
355 dengue viruses only occurs at certain concentrations of mAb (5). While many human
356 tissues express either DPP4 or Fc receptor, a few of them, most notably placenta, express

357 both of them (53, 54). For other viruses that use viral receptors different from DPP4,
358 there may also be human tissues whether the viral receptor and Fc receptor are both
359 expressed. The expression levels of these two receptors in specific tissue cells likely are
360 determinants of mAb dosages at which ADE would occur in these tissues. Other
361 determinants of ADE-enabling mAb dosages may include the binding affinities of the
362 mAb for the viral and Fc receptors. Overall, our study suggests that ADE of viruses
363 depends on antibody dosages, tissue-specific expressions of viral and Fc receptors, and
364 some intrinsic features of the antibody.

365 Our findings not only reveal a novel molecular mechanism for ADE of
366 coronaviruses, but also provide general guidelines on viral vaccine design and antibody-
367 based antiviral drug therapy. As we have shown here, RBD-specific neutralizing mAbs
368 may mediate ADE of viruses by mimicking the functions of viral receptors. Neutralizing
369 mAbs targeting other parts of viral spikes would be less likely to mediate ADE if they do
370 not trigger the conformational changes of the spikes. Hence, to reduce the likelihood of
371 ADE, spike-based subunit vaccines lacking the RBD can be designed to prevent viral
372 infections. Based on the same principle, neutralizing mAbs targeting other parts of the
373 spike can be selected to treat viral infections. Moreover, as already discussed, our study
374 stresses on the importance of choosing antibody dosages that do not cause ADE and
375 points out that different tissue cells should be closely monitored for potential ADE at
376 certain antibody dosages.

377 The *in vitro* systems used in this study provide a model framework for ADE.
378 Future research using *in vivo* systems is needed to further confirm these results. Our
379 previous study showed that a humanized version of Mersmab1 efficiently protected

380 human DPP4-transgenic mice from live MERS-CoV challenges (48, 55), suggesting that
381 given the antibody dosages used in this previous study as well as the binding affinity of
382 the mAb for human DPP4, the receptor-dependent pathway of MERS-CoV entry
383 dominated over ADE *in vivo*. Thus, future *in vivo* studies may need to screen for a wide
384 range of antibody dosages and also for a variety of tissues with different ratios of DPP4
385 and Fc receptor expressions. Although ADE has not been observed for MERS-CoV *in*
386 *vivo*, our study suggests that ADE occurs under some specific conditions *in vivo*,
387 depending on the antibody dosages, binding affinity of the mAb for DPP4, and tissue
388 expressions of DPP4 and Fc receptor. Moreover, the mechanism that we have identified
389 for ADE of MERS-CoV *in vitro* may account for the ADE observed *in vivo* for other
390 coronaviruses such as SARS-CoV and feline coronavirus (42-47). Overall, our study
391 reveals complex roles of antibodies in viral entry and can guide future vaccine design and
392 antibody-based drug therapy.
393

394 **Acknowledgements**

395 We thank Dr. Matthew Aliota for comments. This work was supported by
396 R01AI089728 (to F.L), R01AI110700 (to F.L.), and R01AI139092 (to L.D. and F.L.).

397

398

399 **Materials and Methods**

400 *Cell lines and Plasmids*

401 HEK293T cells and HEK293F cells (human embryonic kidney cells), Hela cells
402 (human cervical cells), and MRC5 cells (human lung cells) were obtained from the
403 ATCC (American Type Culture Collection). HEK293-gamma chain cells (human
404 embryonic kidney cells) were constructed previously (56). These cells were cultured in
405 Dulbecco's modified Eagle medium (DMEM) supplemented with 10% fetal bovine
406 serum (FBS), 2 mM L-glutamine, 100 units/ml penicillin, and 100 µg/ml streptomycin.
407 THP-1 cells (human macrophage cells) were obtained from the ATCC and were cultured
408 in Roswell Park Memorial Institute (RPMI) culture medium (Invitrogen) containing 10%
409 of heat inactivated fetal bovine serum and supplemented with 10 mM Hepes, 1 mM
410 pyruvate, 2.5 g/l D-glucose, 50 pM β-mercaptoethanol, and 100 µg/ml streptomycin.

411 For induction of macrophages, human monocytic THP-1 cells were treated with
412 150 nM phorbol 12-myristate 13-acetate for 24 hours, followed by 24 hours incubation in
413 RPMI medium (57) before experiments.

414 The full-length genes of MERS-CoV spike (GenBank accession number
415 AFS88936.1), SARS-CoV spike (GenBank accession number AFR58742), human DPP4
416 (GenBank accession number NM_001935.3) and human ACE2 (GenBank accession
417 number NM_021804) were synthesized (GenScript Biotech). Three Fc receptor genes,
418 human CD16A (GenBank accession number NM_000569.7), human CD32A (GenBank
419 accession number NM_001136219.1) and human CD64A (GenBank accession number
420 NM_000566.3), were cloned previously (58, 59). For protein expressions on cell surfaces

421 or pseudovirus surfaces, the above genes were subcloned into the pcDNA3.1(+) vector
422 (Life Technologies) with a C-terminal C9 tag.

423 *Protein purification and antibody preparation*

424 For ELISA and negative-stain electron microscopic study, recombinant MERS-
425 CoV spike ectodomain (S-e) was prepared. The MERS-CoV S-e (residues 1-1294) was
426 subcloned into pCMV vector; it contained a C-terminal GCN4 trimerization tag and a
427 His₆ tag. To stabilize S-e in the pre-fusion conformation, we followed the procedure from
428 a previous study by introducing mutations to the S1/S2 protease cleavage site (RSVR748-
429 751ASVA) and the S2 region (V1060P, L1061P) (21). MERS-CoV S-e was expressed in
430 HEK293F cells using a FreeStyle 293 mammalian cell expression system (Life
431 technologies). Briefly, HEK293F cells were transfected with the plasmid encoding
432 MERS-CoV S-e and cultured for three days. The protein was harvested from the cell
433 culture medium, purified sequentially on Ni-NTA column and Superdex200 gel filtration
434 column (GE Healthcare), and stored in a buffer containing 20 mM Tris pH7.2 and 200
435 mM NaCl. The ectodomain of human DPP4 was expressed and purified as previously
436 described (39). Briefly, DPP4 ectodomain (residues 39-766) containing an N-terminal
437 human CD5 signal peptide and a C-terminal His₆ tag were expressed in insect cells using
438 the Bac-to-Bac expression system (Life Technologies), secreted to cell culture medium
439 and purified in the same way as MERS-CoV S-e.

440 Both the MERS-CoV-RBD-specific mAb (i.e., Mersmab1) and SARS-CoV-RBD-
441 specific mAb (i.e., 33G4) were purified as previously described (48, 49). Briefly,
442 hybridoma cells expressing the mAb were injected into the abdomen of mice. After 7-10
443 days, the mouse ascites containing the mAb were collected. The mAb was then purified

444 using a Protein A column (GE Healthcare). Fab of Mersmab1 antibody was prepared
445 using Immobilized Papain beads (ThermoFisher Scientific) according to the
446 manufacturer's manual. Briefly, Mersmab1 antibody was incubated with Immobilized
447 Papain beads in digestion buffer (20 mM sodium phosphate, 10 mM EDTA, 20 mM L-
448 cysteine.HCl pH 7.0) in a shaker water bath at 37 °C overnight. After digestion, the
449 reaction was stopped with 10 mM Tris.HCl pH 7.5, and the supernatant was collected
450 through centrifugation at 12,000g for 15 min. Fab was then separated from undigested
451 IgG and Fc using a Protein A column (GE HealthCare).

452 *ELISA*

453 The binding affinity between mAb and MERS-CoV S-e or RBD was measured
454 using ELISA assay as previously described (60). Briefly, ELISA plates were pre-coated
455 with mAb (350 nM) at 37 °C for 1 hour. After blocking with 1% BSA at 37 °C for 1
456 hour, MERS-CoV S-e or RBD (300 nM or gradient concentrations as specified in Fig. 2)
457 was added to the plates and incubated with mAb at 37 °C for 1 hour. After washes with
458 PBS buffer, the plates were incubated with anti-His₆ antibody (Santa Cruz) at 37 °C for 1
459 hour. Then the plates were washed with PBS and incubated with HRP-conjugated goat
460 anti-mouse IgG antibody (1:5,000) at 37 °C for 1 hour. After more washes with PBS,
461 enzymatic reaction was carried out using ELISA substrate (Life Technologies) and
462 stopped with 1 M H₂SO₄. Absorbance at 450 nm (A450) was measured using Tecan
463 Infinite M1000 PRO Microplate Reader (Tecan Group Ltd.). Five replicates were done
464 for each sample. PBS buffer was used as a negative control.

465 *Flow cytometry cell-binding assay*

466 Flow cytometry was performed as previously described (22). Briefly, HEK293T
467 cells exogenously expressing DPP4 or one of the Fc receptors were incubated with
468 MERS-CoV S-e (40 µg/ml) and mAb (50 µg/ml) (both of which contained a C-terminal
469 His₆ tag) at room temperature for 30 min, followed by incubation with fluorescein
470 phycoerythrin (PE)-labeled anti-His₆ probe antibody for another 30 min. The cells then
471 were analyzed using FACS (fluorescence activated cell sorting).

472 *Pseudovirus entry assay*

473 Coronavirus-spike-mediated pseudovirus entry assay was carried out as
474 previously described (61, 62). Briefly, for pseudovirus packaging, HEK293T cells were
475 co-transfected with a plasmid carrying an Env-defective, luciferase-expressing HIV, type
476 1 genome (pNL4-3.luc.R-E-) and a plasmid encoding MERS-CoV or SARS-CoV spike.
477 Pseudoviruses were harvested and purified using a sucrose gradient ultracentrifugation at
478 40,000g 72 hours after transfection and then used to enter the target cells. To detect
479 pseudovirus entry, pseudoviruses and cells were incubated for 5 hours at 37°C, and then
480 medium was changed and cells were incubated for an additional 60 hours. Cells were
481 then washed with PBS and lysed. Aliquots of cell lysates were transferred to Optiplate-96
482 (PerkinElmer), followed by addition of luciferase substrate. Relative light unites (RLUs)
483 were measured using EnSpire plate reader (PerkinElmer). All the measurements were
484 carried out in four replicates. To inhibit proprotein convertases during packaging of
485 MERS-CoV pseudoviruses, 50 nM proprotein convertase inhibitor (PPCi) Dec-RVKR-
486 CMK (Enzo Life Sciences) was added to the cell culture medium 5 hours post
487 transfection, before the packaged pseudoviruses were purified as described above.
488 Inhibition of pseudovirus entry using various protease inhibitors was carried out as

489 described previously (63). Briefly, cells were pre-treated with 50 nM proprotein
490 convertase inhibitor Dec-RVKR-CMK (Enzo Life Sciences), 100 nM camostat mesylate
491 (Sigma-Aldrich), 100 nM bafilomycin A1 (Baf-A1) (Sigma-Aldrich), 50 nM E64d
492 (Sigma-Aldrich), at 37 °C for 1 hour, or 500 ng/ml antibody for 5 min. The above cells
493 were then used for pseudovirus entry assay.

494 *Isolation and quantification of cell surface receptor proteins*

495 To examine the expression levels of receptor proteins in cell membranes, the cells
496 expressing the receptor were harvested and all membrane-associated proteins were
497 extracted using a membrane protein extraction kit (Thermo Fisher Scientific). Briefly,
498 cells were centrifuged at 300g for 5 min and washed with cell wash solution twice. The
499 cell pellets were resuspended in 0.75 ml permeabilization buffer and incubated at 4°C for
500 10 min. The supernatant containing cytosolic proteins was removed after centrifugation at
501 16,000g for 15 min. The pellets containing membrane-associated proteins were
502 resuspended in 0.5 ml solubilization buffer and incubated at 4°C for 30 min. After
503 centrifugation at 16,000g for 15 min, the membrane-associated proteins from the
504 supernatant were transferred to a new tube. The expression level of membrane-associated
505 C9-tagged receptor proteins among all membrane-associated proteins was then measured
506 using Western blot analysis and further used for normalizing the results from flow
507 cytometry cell-binding assays and pseudovirus entry assays.

508 *Extraction of total RNA and qRT-PCR*

509 Total RNAs of cells were extracted using TRIzol reagent according to the
510 manufacturer's manual. Briefly, TRIzol was added to the cell lysate, and then chloroform
511 and phenol-chloroform were added to precipitate RNA. The RNA pellets were washed

512 using ethanol, solubilized in DEPC-treated water, and then reverse-transcribed using
513 MLV reverse transcriptase (Promega) and oligo dT primers (Promega). Quantitative PCR
514 on DPP4 RNA was performed using DPP4-specific primers and SYBR qPCR kit (Bio-
515 Rad) in CFX qPCR instrument (Bio-Rad). Glyceraldehyde 3-phosphate dehydrogenase
516 (GAPDH) RNA was used as a control. The primers are listed below:

517 DPP4 - forward-5'-AGTGGCGTGTTC AAGTGTGG-3'; reverse-5'-

518 CAAGGTTGTCTTCTGGAGTTGG-3'

519 GAPDH - forward-5'-GGAAGGTGAAGGTCGGAGTCAACGG-3'; reverse-5'-

520 CTCGCTCCTGGAAGATGGTGATGGG-3'

521 *Proteolysis assay*

522 Purified MERS-CoV pseudoviruses were incubated with 67 µg/ml recombinant
523 DPP4, 67 µg/ml mAb or PBS at 37 °C for 30 min, and then treated with 10⁻³ mg/ml
524 TPCK-treated-trypsin on ice for 20 min. Samples were subjected to Western blotting
525 analysis. MERS-CoV spike and its cleaved fragments (which contained a C-terminal C9
526 tag) were detected using an anti-C9 tag monoclonal antibody (Santa Cruz
527 Biotechnology).

528 *Negative-stain electron microscopy*

529 Samples were diluted to a final concentration of 0.02 mg/mL in PBS buffer and
530 loaded onto glow-discharged 400 mesh carbon grids (Electron Microscopy Sciences).
531 The grids were stained with 0.75% uranyl formate. All micrographs were acquired using
532 a Tecnai G2 Spirit BioTWIN at 120 keV (FEI Company) and an Eagle 4 mega pixel CCD
533 camera at 6,000 × nominal magnification at the University of Minnesota.

534

535

536 **References**

537

538 1. **Tirado SM, Yoon KJ.** 2003. Antibody-dependent enhancement of virus infection
539 and disease. *Viral Immunol* **16**:69-86.

540

541 2. **Takada A, Kawaoka Y.** 2003. Antibody-dependent enhancement of viral
542 infection: molecular mechanisms and in vivo implications. *Rev Med Virol*
13:387-398.

543

544 3. **Guzman MG, Alvarez M, Rodriguez-Roche R, Bernardo L, Montes T,**
545 **Vazquez S, Morier L, Alvarez A, Gould EA, Kouri G, Halstead SB.** 2007.
546 Neutralizing antibodies after infection with dengue 1 virus. *Emerg Infect Dis*
13:282-286.

547

548 4. **Dejnirattisai W, Jumnainsong A, Onsirisakul N, Fitton P, Vasanawathana S,**
549 **Limpitikul W, Puttikhunt C, Edwards C, Duangchinda T, Supasa S,**
550 **Chawansuntati K, Malasit P, Mongkolsapaya J, Screaton G.** 2010. Cross-
551 reacting antibodies enhance dengue virus infection in humans. *Science* **328**:745-
748.

552

553 5. **Katzelnick LC, Gresh L, Halloran ME, Mercado JC, Kuan G, Gordon A,**
554 **Balmaseda A, Harris E.** 2017. Antibody-dependent enhancement of severe
dengue disease in humans. *Science* **358**:929-932.

555

556 6. **Whitehead SS, Blaney JE, Durbin AP, Murphy BR.** 2007. Prospects for a
dengue virus vaccine. *Nat Rev Microbiol* **5**:518-528.

557

558 7. **Wiley S, Aasa-Chapman MM, O'Farrell S, Pellegrino P, Williams I, Weiss**
559 **RA, Neil SJ.** 2011. Extensive complement-dependent enhancement of HIV-1 by
560 autologous non-neutralising antibodies at early stages of infection. *Retrovirology*
8:16.

561

562 8. **Beck Z, Prohaszka Z, Fust G.** 2008. Traitors of the immune system-enhancing
563 antibodies in HIV infection: their possible implication in HIV vaccine
development. *Vaccine* **26**:3078-3085.

564

565 9. **Takada A, Watanabe S, Okazaki K, Kida H, Kawaoka Y.** 2001. Infectivity-
enhancing antibodies to Ebola virus glycoprotein. *J Virol* **75**:2324-2330.

566

567 10. **Takada A, Feldmann H, Ksiazek TG, Kawaoka Y.** 2003. Antibody-dependent
enhancement of Ebola virus infection. *J Virol* **77**:7539-7544.

568

569 11. **Perlman S, Netland J.** 2009. Coronaviruses post-SARS: update on replication
and pathogenesis. *Nature Reviews Microbiology* **7**:439-450.

- 570 12. **Enjuanes L, Almazan F, Sola I, Zuniga S.** 2006. Biochemical aspects of
571 coronavirus replication and virus-host interaction. *Annu Rev Microbiol* **60**:211-
572 230.
- 573 13. **Zaki AM, van Boheemen S, Bestebroer TM, Osterhaus A, Fouchier RAM.**
574 2012. Isolation of a Novel Coronavirus from a Man with Pneumonia in Saudi
575 Arabia. *New England Journal of Medicine* **367**:1814-1820.
- 576 14. **Ksiazek TG, Erdman D, Goldsmith CS, Zaki SR, Peret T, Emery S, Tong**
577 **SX, Urbani C, Comer JA, Lim W, Rollin PE, Dowell SF, Ling AE,**
578 **Humphrey CD, Shieh WJ, Guarner J, Paddock CD, Rota P, Fields B, DeRisi**
579 **J, Yang JY, Cox N, Hughes JM, LeDuc JW, Bellini WJ, Anderson LJ.** 2003.
580 A novel coronavirus associated with severe acute respiratory syndrome. *New*
581 *England Journal of Medicine* **348**:1953-1966.
- 582 15. **Peiris JSM, Lai ST, Poon LLM, Guan Y, Yam LYC, Lim W, Nicholls J, Yee**
583 **WKS, Yan WW, Cheung MT, Cheng VCC, Chan KH, Tsang DNC, Yung**
584 **RWH, Ng TK, Yuen KY.** 2003. Coronavirus as a possible cause of severe acute
585 respiratory syndrome. *Lancet* **361**:1319-1325.
- 586 16. **de Groot RJ, Baker SC, Baric RS, Brown CS, Drosten C, Enjuanes L,**
587 **Fouchier RA, Galiano M, Gorbalenya AE, Memish ZA, Perlman S, Poon LL,**
588 **Snijder EJ, Stephens GM, Woo PC, Zaki AM, Zambon M, Ziebuhr J.** 2013.
589 Middle East respiratory syndrome coronavirus (MERS-CoV): announcement of
590 the Coronavirus Study Group. *J Virol* **87**:7790-7792.
- 591 17. **Li F.** 2016. Structure, Function, and Evolution of Coronavirus Spike Proteins.
592 *Annu Rev Virol* **3**:237-261.
- 593 18. **Yuan Y, Cao D, Zhang Y, Ma J, Qi J, Wang Q, Lu G, Wu Y, Yan J, Shi Y,**
594 **Zhang X, Gao GF.** 2017. Cryo-EM structures of MERS-CoV and SARS-CoV
595 spike glycoproteins reveal the dynamic receptor binding domains. *Nat Commun*
596 **8**:15092.
- 597 19. **Shang J, Zheng Y, Yang Y, Liu C, Geng Q, Luo C, Zhang W, Li F.** 2018.
598 Cryo-EM structure of infectious bronchitis coronavirus spike protein reveals
599 structural and functional evolution of coronavirus spike proteins. *PLoS Pathog*
600 **14**:e1007009.
- 601 20. **Song W, Gui M, Wang X, Xiang Y.** 2018. Cryo-EM structure of the SARS
602 coronavirus spike glycoprotein in complex with its host cell receptor ACE2. *PLoS*
603 *Pathog* **14**:e1007236.
- 604 21. **Pallesen J, Wang N, Corbett KS, Wrapp D, Kirchdoerfer RN, Turner HL,**
605 **Cottrell CA, Becker MM, Wang L, Shi W, Kong WP, Andres EL,**
606 **Kettenbach AN, Denison MR, Chappell JD, Graham BS, Ward AB,**
607 **McLellan JS.** 2017. Immunogenicity and structures of a rationally designed

- 608 prefusion MERS-CoV spike antigen. Proc Natl Acad Sci U S A **114**:E7348-
609 e7357.
- 610 22. **Shang J, Zheng Y, Yang Y, Liu C, Geng Q, Tai W, Du L, Zhou Y, Zhang W,**
611 **Li F.** 2018. Cryo-Electron Microscopy Structure of Porcine Deltacoronavirus
612 Spike Protein in the Prefusion State. J Virol **92**.
- 613 23. **Walls AC, Tortorici MA, Bosch BJ, Frenz B, Rottier PJ, DiMaio F, Rey FA,**
614 **Veesler D.** 2016. Cryo-electron microscopy structure of a coronavirus spike
615 glycoprotein trimer. Nature **531**:114-117.
- 616 24. **Walls AC, Tortorici MA, Frenz B, Snijder J, Li W, Rey FA, DiMaio F, Bosch**
617 **BJ, Veesler D.** 2016. Glycan shield and epitope masking of a coronavirus spike
618 protein observed by cryo-electron microscopy. Nat Struct Mol Biol **23**:899-905.
- 619 25. **Kirchdoerfer RN, Cottrell CA, Wang N, Pallesen J, Yassine HM, Turner HL,**
620 **Corbett KS, Graham BS, McLellan JS, Ward AB.** 2016. Pre-fusion structure
621 of a human coronavirus spike protein. Nature **531**:118-121.
- 622 26. **Li F.** 2015. Receptor recognition mechanisms of coronaviruses: a decade of
623 structural studies. J Virol **89**:1954-1964.
- 624 27. **Li WH, Moore MJ, Vasilieva N, Sui JH, Wong SK, Berne MA,**
625 **Somasundaran M, Sullivan JL, Luzuriaga K, Greenough TC, Choe H,**
626 **Farzan M.** 2003. Angiotensin-converting enzyme 2 is a functional receptor for
627 the SARS coronavirus. Nature **426**:450-454.
- 628 28. **Raj VS, Mou HH, Smits SL, Dekkers DHW, Muller MA, Dijkman R, Muth**
629 **D, Demmers JAA, Zaki A, Fouchier RAM, Thiel V, Drosten C, Rottier PJM,**
630 **Osterhaus A, Bosch BJ, Haagmans BL.** 2013. Dipeptidyl peptidase 4 is a
631 functional receptor for the emerging human coronavirus-EMC. Nature **495**:251-
632 254.
- 633 29. **Li F, Li WH, Farzan M, Harrison SC.** 2005. Structure of SARS coronavirus
634 spike receptor-binding domain complexed with receptor. Science **309**:1864-1868.
- 635 30. **Lu G, Hu Y, Wang Q, Qi J, Gao F, Li Y, Zhang Y, Zhang W, Yuan Y, Bao J,**
636 **Zhang B, Shi Y, Yan J, Gao GF.** 2013. Molecular basis of binding between
637 novel human coronavirus MERS-CoV and its receptor CD26. Nature **500**:227-
638 231.
- 639 31. **Belouzard S, Millet JK, Licitra BN, Whittaker GR.** 2012. Mechanisms of
640 coronavirus cell entry mediated by the viral spike protein. Viruses **4**:1011-1033.
- 641 32. **Heald-Sargent T, Gallagher T.** 2012. Ready, set, fuse! The coronavirus spike
642 protein and acquisition of fusion competence. Viruses **4**:557-580.

- 643 33. **Bertram S, Glowacka I, Muller MA, Lavender H, Gnirss K, Nehlmeier I,**
644 **Niemeyer D, He Y, Simmons G, Drosten C, Soilleux EJ, Jahn O, Steffen I,**
645 **Pohlmann S.** 2011. Cleavage and activation of the severe acute respiratory
646 syndrome coronavirus spike protein by human airway trypsin-like protease. *J*
647 *Virol* **85**:13363-13372.
- 648 34. **Matsuyama S, Ujike M, Morikawa S, Tashiro M, Taguchi F.** 2005. Protease-
649 mediated enhancement of severe acute respiratory syndrome coronavirus
650 infection. *Proceedings of the National Academy of Sciences of the United States*
651 *of America* **102**:12543-12547.
- 652 35. **Kam YW, Okumura Y, Kido H, Ng LF, Bruzzone R, Altmeyer R.** 2009.
653 Cleavage of the SARS coronavirus spike glycoprotein by airway proteases
654 enhances virus entry into human bronchial epithelial cells in vitro. *PLoS One*
655 **4**:e7870.
- 656 36. **Shirato K, Kawase M, Matsuyama S.** 2013. Middle East respiratory syndrome
657 coronavirus infection mediated by the transmembrane serine protease TMPRSS2.
658 *J Virol* **87**:12552-12561.
- 659 37. **Gierer S, Muller MA, Heurich A, Ritz D, Springstein BL, Karsten CB,**
660 **Schendzielorz A, Gnirss K, Drosten C, Pohlmann S.** 2015. Inhibition of
661 proprotein convertases abrogates processing of the middle eastern respiratory
662 syndrome coronavirus spike protein in infected cells but does not reduce viral
663 infectivity. *J Infect Dis* **211**:889-897.
- 664 38. **Gierer S, Bertram S, Kaup F, Wrensch F, Heurich A, Kramer-Kuhl A,**
665 **Welsch K, Winkler M, Meyer B, Drosten C, Dittmer U, von Hahn T,**
666 **Simmons G, Hofmann H, Pohlmann S.** 2013. The spike protein of the emerging
667 betacoronavirus EMC uses a novel coronavirus receptor for entry, can be
668 activated by TMPRSS2, and is targeted by neutralizing antibodies. *J Virol*
669 **87**:5502-5511.
- 670 39. **Zheng Y, Shang J, Yang Y, Liu C, Wan Y, Geng Q, Wang M, Baric R, Li F.**
671 2018. Lysosomal Proteases Are a Determinant of Coronavirus Tropism. *J Virol*
672 **92**.
- 673 40. **Walls AC, Tortorici MA, Snijder J, Xiong X, Bosch BJ, Rey FA, Veasler D.**
674 2017. Tectonic conformational changes of a coronavirus spike glycoprotein
675 promote membrane fusion. *Proc Natl Acad Sci U S A* **114**:11157-11162.
- 676 41. **Li F, Berardi M, Li WH, Farzan M, Dormitzer PR, Harrison SC.** 2006.
677 Conformational states of the severe acute respiratory syndrome coronavirus spike
678 protein ectodomain. *Journal of Virology* **80**:6794-6800.
- 679 42. **Wang SF, Tseng SP, Yen CH, Yang JY, Tsao CH, Shen CW, Chen KH, Liu**
680 **FT, Liu WT, Chen YM, Huang JC.** 2014. Antibody-dependent SARS

- 681 coronavirus infection is mediated by antibodies against spike proteins. *Biochem*
682 *Biophys Res Commun* **451**:208-214.
- 683 43. **Kam YW, Kien F, Roberts A, Cheung YC, Lamirande EW, Vogel L, Chu**
684 **SL, Tse J, Guarner J, Zaki SR, Subbarao K, Peiris M, Nal B, Altmeyer R.**
685 2007. Antibodies against trimeric S glycoprotein protect hamsters against SARS-
686 CoV challenge despite their capacity to mediate Fcγ₂RII-dependent entry
687 into B cells in vitro. *Vaccine* **25**:729-740.
- 688 44. **Jaume M, Yip MS, Cheung CY, Leung HL, Li PH, Kien F, Dutry I,**
689 **Callendret B, Escriou N, Altmeyer R, Nal B, Daeron M, Bruzzone R, Peiris**
690 **JS.** 2011. Anti-severe acute respiratory syndrome coronavirus spike antibodies
691 trigger infection of human immune cells via a pH- and cysteine protease-
692 independent Fcγ₂R pathway. *J Virol* **85**:10582-10597.
- 693 45. **Corapi WV, Olsen CW, Scott FW.** 1992. Monoclonal antibody analysis of
694 neutralization and antibody-dependent enhancement of feline infectious
695 peritonitis virus. *J Virol* **66**:6695-6705.
- 696 46. **Hohdatsu T, Yamada M, Tominaga R, Makino K, Kida K, Koyama H.** 1998.
697 Antibody-dependent enhancement of feline infectious peritonitis virus infection in
698 feline alveolar macrophages and human monocyte cell line U937 by serum of cats
699 experimentally or naturally infected with feline coronavirus. *J Vet Med Sci* **60**:49-
700 55.
- 701 47. **Vennema H, de Groot RJ, Harbour DA, Dalderup M, Gruffydd-Jones T,**
702 **Horzinek MC, Spaan WJ.** 1990. Early death after feline infectious peritonitis
703 virus challenge due to recombinant vaccinia virus immunization. *J Virol* **64**:1407-
704 1409.
- 705 48. **Du L, Zhao G, Yang Y, Qiu H, Wang L, Kou Z, Tao X, Yu H, Sun S, Tseng**
706 **CT, Jiang S, Li F, Zhou Y.** 2014. A Conformation-Dependent Neutralizing
707 Monoclonal Antibody Specifically Targeting Receptor-Binding Domain in
708 Middle East Respiratory Syndrome Coronavirus Spike Protein. *J Virol* **88**:7045-
709 7053.
- 710 49. **Du L, Zhao G, Li L, He Y, Zhou Y, Zheng BJ, Jiang S.** 2009. Antigenicity and
711 immunogenicity of SARS-CoV S protein receptor-binding domain stably
712 expressed in CHO cells. *Biochem Biophys Res Commun* **384**:486-490.
- 713 50. **He YX, Lu H, Siddiqui P, Zhou YS, Jiang SB.** 2005. Receptor-binding domain
714 of severe acute respiratory syndrome coronavirus spike protein contains multiple
715 conformation-dependent epitopes that induce highly potent neutralizing
716 antibodies. *Journal of Immunology* **174**:4908-4915.
- 717 51. **Millet JK, Whittaker GR.** 2014. Host cell entry of Middle East respiratory
718 syndrome coronavirus after two-step, furin-mediated activation of the spike
719 protein. *Proc Natl Acad Sci U S A* **111**:15214-15219.

- 720 52. **Walls AC, Xiong X, Park YJ, Tortorici MA, Snijder J, Quispe J, Cameroni**
721 **E, Gopal R, Dai M, Lanzavecchia A, Zambon M, Rey FA, Corti D, Veesler D.**
722 2019. Unexpected Receptor Functional Mimicry Elucidates Activation of
723 Coronavirus Fusion. *Cell* **176**:1026-1039.e1015.
- 724 53. **Uhlen M, Fagerberg L, Hallstrom BM, Lindskog C, Oksvold P, Mardinoglu**
725 **A, Sivertsson A, Kampf C, Sjostedt E, Asplund A, Olsson I, Edlund K,**
726 **Lundberg E, Navani S, Szgyarto CA, Odeberg J, Djureinovic D, Takanen**
727 **JO, Hober S, Alm T, Edqvist PH, Berling H, Tegel H, Mulder J, Rockberg J,**
728 **Nilsson P, Schwenk JM, Hamsten M, von Feilitzen K, Forsberg M, Persson**
729 **L, Johansson F, Zwahlen M, von Heijne G, Nielsen J, Ponten F.** 2015.
730 Proteomics. Tissue-based map of the human proteome. *Science* **347**:1260419.
- 731 54. **Uhlen M, Bjorling E, Agaton C, Szgyarto CA, Amini B, Andersen E,**
732 **Andersson AC, Angelidou P, Asplund A, Asplund C, Berglund L, Bergstrom**
733 **K, Brumer H, Cerjan D, Ekstrom M, Elobeid A, Eriksson C, Fagerberg L,**
734 **Falk R, Fall J, Forsberg M, Bjorklund MG, Gumbel K, Halimi A, Hallin I,**
735 **Hamsten C, Hansson M, Hedhammar M, Hercules G, Kampf C, Larsson K,**
736 **Lindskog M, Lodewyckx W, Lund J, Lundeberg J, Magnusson K, Malm E,**
737 **Nilsson P, Odling J, Oksvold P, Olsson I, Oster E, Ottosson J, Paavilainen L,**
738 **Persson A, Rimini R, Rockberg J, Runeson M, Sivertsson A, Skolleremo A, et**
739 **al.** 2005. A human protein atlas for normal and cancer tissues based on antibody
740 proteomics. *Mol Cell Proteomics* **4**:1920-1932.
- 741 55. **Qiu H, Sun S, Xiao H, Feng J, Guo Y, Tai W, Wang Y, Du L, Zhao G, Zhou**
742 **Y.** 2016. Single-dose treatment with a humanized neutralizing antibody affords
743 full protection of a human transgenic mouse model from lethal Middle East
744 respiratory syndrome (MERS)-coronavirus infection. *Antiviral Res* **132**:141-148.
- 745 56. **Jing Y, Ni Z, Wu J, Higgins L, Markowski TW, Kaufman DS, Walcheck B.**
746 2015. Identification of an ADAM17 cleavage region in human CD16
747 (FcγRIII) and the engineering of a non-cleavable version of the receptor in
748 NK cells. *PLoS One* **10**:e0121788.
- 749 57. **Genin M, Clement F, Fattaccioli A, Raes M, Michiels C.** 2015. M1 and M2
750 macrophages derived from THP-1 cells differentially modulate the response of
751 cancer cells to etoposide. *BMC Cancer* **15**:577.
- 752 58. **Snyder KM, Hullsiek R, Mishra HK, Mendez DC, Li Y, Rogich A, Kaufman**
753 **DS, Wu J, Walcheck B.** 2018. Expression of a Recombinant High Affinity IgG
754 Fc Receptor by Engineered NK Cells as a Docking Platform for Therapeutic
755 mAbs to Target Cancer Cells. *Front Immunol* **9**:2873.
- 756 59. **Su K, Li X, Edberg JC, Wu J, Ferguson P, Kimberly RP.** 2004. A promoter
757 haplotype of the immunoreceptor tyrosine-based inhibitory motif-bearing
758 FcγRIIb alters receptor expression and associates with autoimmunity. II.

- 759 Differential binding of GATA4 and Yin-Yang1 transcription factors and
760 correlated receptor expression and function. *J Immunol* **172**:7192-7199.
- 761 60. **Du L, Tai W, Yang Y, Zhao G, Zhu Q, Sun S, Liu C, Tao X, Tseng CK,**
762 **Perlman S, Jiang S, Zhou Y, Li F.** 2016. Introduction of neutralizing
763 immunogenicity index to the rational design of MERS coronavirus subunit
764 vaccines. *Nat Commun* **7**:13473.
- 765 61. **Liu C, Tang J, Ma Y, Liang X, Yang Y, Peng G, Qi Q, Jiang S, Li J, Du L, Li**
766 **F.** 2015. Receptor usage and cell entry of porcine epidemic diarrhea coronavirus.
767 *J Virol* **89**:6121-6125.
- 768 62. **Yang Y, Du L, Liu C, Wang L, Ma C, Tang J, Baric RS, Jiang S, Li F.** 2014.
769 Receptor usage and cell entry of bat coronavirus HKU4 provide insight into bat-
770 to-human transmission of MERS coronavirus. *Proc Natl Acad Sci U S A*
771 **111**:12516-12521.
- 772 63. **Liu C, Ma Y, Yang Y, Zheng Y, Shang J, Zhou Y, Jiang S, Du L, Li J, Li F.**
773 2016. Cell Entry of Porcine Epidemic Diarrhea Coronavirus Is Activated by
774 Lysosomal Proteases. *J Biol Chem* **291**:24779-24786.
- 775 64. **Chen Y, Rajashankar KR, Yang Y, Agnihothram SS, Liu C, Lin YL, Baric**
776 **RS, Li F.** 2013. Crystal structure of the receptor-binding domain from newly
777 emerged Middle East respiratory syndrome coronavirus. *J Virol* **87**:10777-10783.
778

779 **Figure Legends:**

780 **Figure 1.** Structural similarity between DPP4 and mAb in binding MERS-CoV spike. (A)

781 Tertiary structure of MERS-CoV RBD in complex with DPP4 (PDB code: 4KR0) (30).

782 DPP4 is colored yellow. RBD is colored cyan (core structure) and red (receptor-binding

783 motif). DPP4 binds to the receptor-binding motif of the RBD. (B) Modeled structure of

784 MERS-CoV S-e in complex with DPP4. S-e is a trimer (PDB code: 5X5F): one

785 monomeric subunit whose RBD is in the standing-up conformation is colored blue and

786 the other two monomeric subunits whose RBDs are in the lying-down conformation are

787 colored grey (18). To generate the structural model of the S-e in complex with DPP4, the

788 RBD in panel (A) was structurally aligned with the standing-up RBD in the S-e trimer.

789 (C) Tertiary structure of MERS-CoV RBD (PDB 4L3N) (64). Critical mAb-binding

790 residues were identified through mutagenesis studies (48) and are shown as green sticks.

791

792 **Figure 2.** Interactions between coronavirus spike and RBD-specific mAb. (A) ELISA for

793 detection of the binding between MERS-CoV-RBD-specific mAb (i.e., Mersmab1) and

794 MERS-CoV spike ectodomain (S-e). Mersmab1 was pre-coated on the plate, and

795 recombinant S-e or RBD was added subsequently for ELISA. Binding affinities were

796 characterized as ELISA signal at OD 450 nm. PBS was used as a negative control. (B)

797 ELISA for detection of the binding between Fab of Mersmab1 and MERS-CoV S-e.

798 Recombinant S-e was pre-coated on the plate, and Mersmab1 or Fab was added

799 subsequently for ELISA. (C) Flow cytometry for detection of the binding between

800 MERS-CoV S-e and DPP4 receptor and among S-e, Mersmab1 and CD32A (i.e., Fc

801 receptor). Cells expressing DPP4 or CD32A were incubated with S-e alone, S-e plus

802 Mersmab1, or S-e plus a SARS-CoV-RBD-specific mAb (i.e., 33G4). Fluorescence-
803 labeled anti-His₆ antibody was added to target the C-terminal His₆ tag on S-e. Cells were
804 analyzed using FACS (fluorescence-activated cell sorting). (D) The expression levels of
805 cell-membrane-associated DPP4 and CD32A were characterized using Western blot
806 targeting their C-terminal C9 tag, and then used to normalize the binding affinity as
807 measured in panel (C). As an internal control, the expression level of cellular actin was
808 measured using an anti-actin antibody. All of the experiments were repeated at least three
809 times with similar results, and representative results are shown here. Error bars indicate
810 S.D. (n=5). Statistical analyses were performed as one-tailed *t*-test. *** $p < 0.001$.

811 Mersmab1 and its Fab both bind to MERS-CoV RBD and S-e.

812

813 **Figure 3.** Antibody-dependent enhancement of coronavirus entry. (A) Antibody-
814 mediated MERS-CoV pseudovirus entry into human cells. The human cells included
815 HEK293T cells exogenously expressing DPP4, HEK293T cells exogenously expressing
816 one of the Fc receptors (CD16A, CD32A, or CD64A), and macrophage cells (induced
817 from THP-1 monocytes cells) endogenously expressing a mixture of Fc receptors. The
818 antibody was Mersmab1. An anti-SARS mAb (i.e., 33G4) was used as a negative control.
819 Efficiency of pseudovirus entry was characterized by luciferase activities accompanying
820 entry. HEK293T cells not expressing any viral receptor or Fc receptor were used as a
821 mock. (B) Fc- or Fab-mediated MERS-CoV pseudovirus entry into human cells. The Fc
822 or the Fab portion of Mersmab1 was used in MERS-CoV pseudovirus entry performed as
823 in panel (A). (C) Expression levels of DPP4 receptor in different cell lines. Total RNA
824 was extracted from three different cell lines: HEK293T, MRC5 and Hela. Then qRT-PCR

825 was performed on the total RNAs from each cell line. The expression level of DPP4 in
826 each cell line is defined as the ratio between the RNA of DPP4 and the RNA of
827 Glyceraldehyde 3-phosphate dehydrogenase (GAPDH). (D) Antibody-mediated MERS-
828 CoV pseudovirus entry into Hela cells that do not express DPP4 receptor. The
829 experiments were performed in the same way as in panel (A), except that Hela cells
830 replaced HEK293T cells. (E) Antibody-mediated SARS-CoV pseudovirus entry into
831 human cells. DPP4 and Mersmab1 were replaced by ACE2 and 33G4, respectively.
832 Mersmab1 was used as a negative control. All of the experiments were repeated at least
833 three times with similar results, and representative results are shown here. Error bars
834 indicate S.D. (n=4). Statistical analyses were performed as one-tailed *t*-test. *** $p <$
835 0.001. RBD-specific mAbs mediate ADE of coronavirus entry, while blocking viral-
836 receptor-dependent coronavirus entry.

837

838 **Figure 4.** Antibody-induced conformational changes of coronavirus spike. (A) Purified
839 MERS-CoV pseudoviruses were incubated with recombinant DPP4, mAb or PBS, and
840 then treated with trypsin. Samples were subjected to Western blotting analysis. MERS-
841 CoV spike and its cleaved fragments (all of which contained a C-terminal C9 tag) were
842 detected using an anti-C9 tag monoclonal antibody. Both DPP4 and Mersmab1 triggered
843 conformational changes of MERS-CoV spike, allowing it to be cleaved at the S2' site by
844 trypsin. (B) Negative-stain electron microscopic analysis of MERS-CoV S-e in complex
845 with the Fab of Mersmab1. Both a field of particles and windows of individual particles
846 are shown. Black arrows indicate S-e-bound Fabs. According to previous studies (18, 20,

847 21), the Fab-binding site on the trimeric S-e is accessible only when the RBD is in the
848 standing-up position.

849 **Figure 5.** Pathways for antibody-dependent enhancement of coronavirus entry. (A)
850 Impact of proprotein convertases on ADE of MERS-CoV entry. During packaging of
851 MERS-CoV pseudoviruses, HEK293T cells were treated with proprotein convertase
852 inhibitor (PPCi). The MERS-CoV pseudoviruses packaged in the presence of PPCi were
853 then subjected to MERS-CoV pseudovirus entry into HEK293T cells expressing either
854 DPP4 receptor or CD32A receptor. (B) Western blot of MERS-CoV pseudoviruses
855 packaged in the presence or absence of PPCi. MERS-CoV spike protein was detected
856 using anti-C9 antibody targeting its C-terminal C9 tag. As an internal control, another
857 viral protein, p24, was detected using anti-p24 antibody. (C) Impact of cell-surface
858 proteases on ADE of MERS-CoV entry. HEK293T cells exogenously expressing
859 TMPRSS2 (which is a common cell-surface protease) were subjected to MERS-CoV
860 pseudovirus entry. TMPRSS2 enhanced both the DPP4-dependent and antibody-
861 dependent entry pathways. (D) Impact of lysosomal proteases on ADE of MERS-CoV
862 entry. HEK293T cells exogenously expressing DPP4 or CD32A were pretreated with one
863 of the lysosomal protease inhibitors, E64d and Baf-A1, and then subjected to MERS-CoV
864 pseudovirus entry. Lysosomal proteases blocked both the DPP4-dependent and antibody-
865 dependent entry pathways. Hence DPP4-dependent and Mersmab1-dependent MERS-
866 CoV entries share the same pathways. HEK293T cells not expressing DPP4 or CD32A
867 were used as a negative control. All of the experiments were repeated at least three times
868 with similar results, and representative results are shown here. Error bars indicate S.D.

869 (n=4). Statistical analyses were performed as one-tailed *t*-test. *** $p < 0.001$. * $p < 0.05$.

870 Antibody-dependent and DPP4-dependent viral entries share the same pathways.

871 **Figure 6.** Antibody dosages for antibody-dependent enhancement of coronavirus entry.

872 (A) Impact of antibody dosages on MERS-CoV pseudovirus entry into HEK293T cells
873 exogenously expressing either DPP4 or CD32A. mAb blocks the DPP4-dependent entry
874 pathway; it enhances the antibody-dependent entry pathway at lower concentrations and
875 blocks it at higher concentrations. (B) Impact of antibody dosages on MERS-CoV

876 pseudovirus entry into HEK293T cells exogenously expressing both DPP4 and CD32A.

877 In the presence of both DPP4 and CD32A, mAb blocks viral entry at low concentrations,
878 enhances viral entry at intermediate concentrations, and blocks viral entry at high

879 concentrations. (C) Same experiment as in panel (A), except that MRC5 cells replaced

880 HEK293T cells. Here MRC5 cells express DPP4 receptor endogenously. (D) Same

881 experiment as in panel (B), except that MRC5 cells replaced HEK293T cells. Here

882 MRC5 cells endogenously express DPP4 and exogenously express CD32A. Please refer

883 to text for more detailed explanations. All of the experiments were repeated at least three

884 times with similar results, and representative results are shown here. Error bars indicate

885 S.D. (n=4).

886 **Figure 7.** Two previously published structures of coronavirus spike proteins complexed

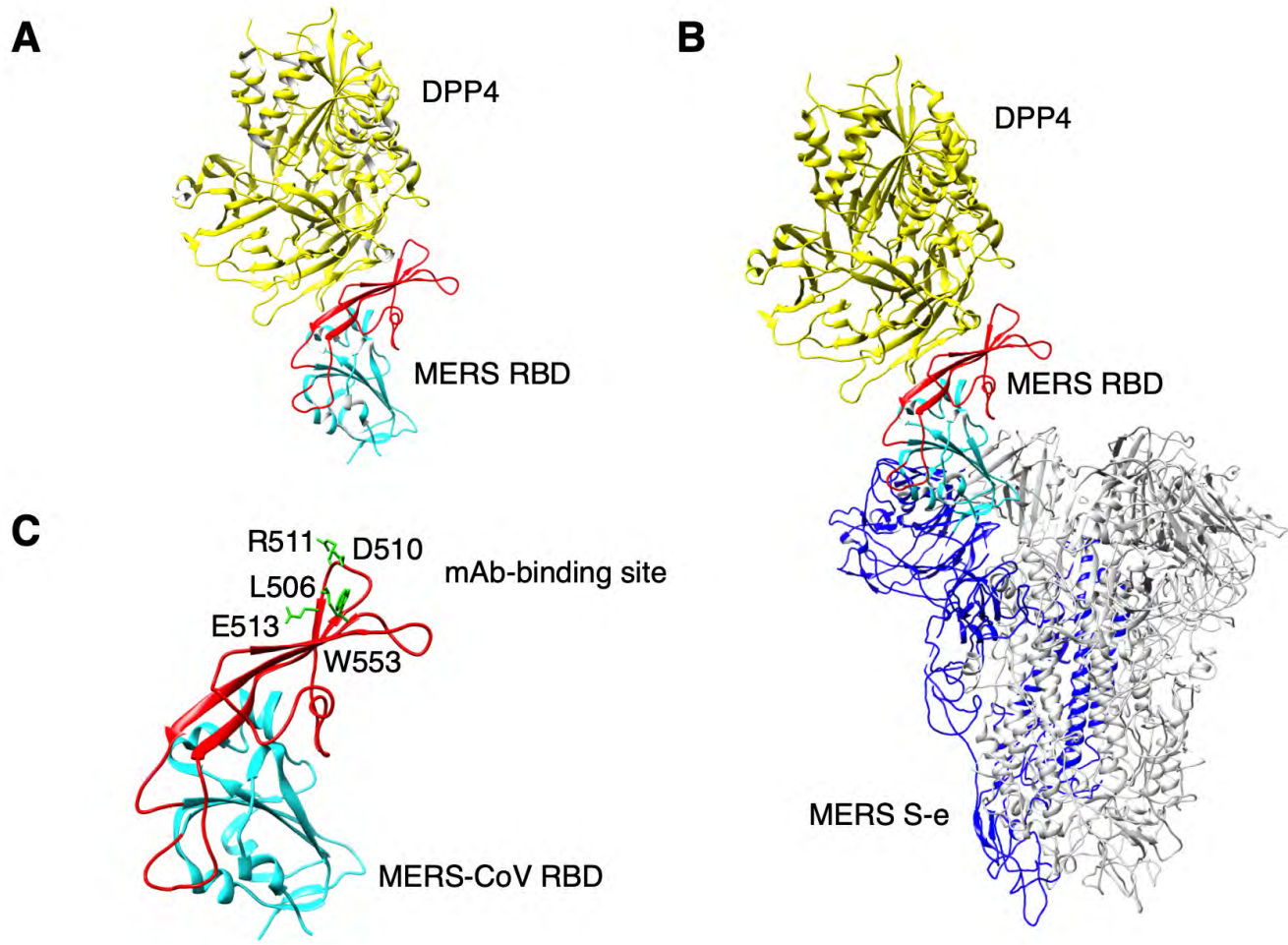
887 with antibody. (A) SARS-CoV S-e complexed with S230 mAb (PDB ID: 6NB7). The

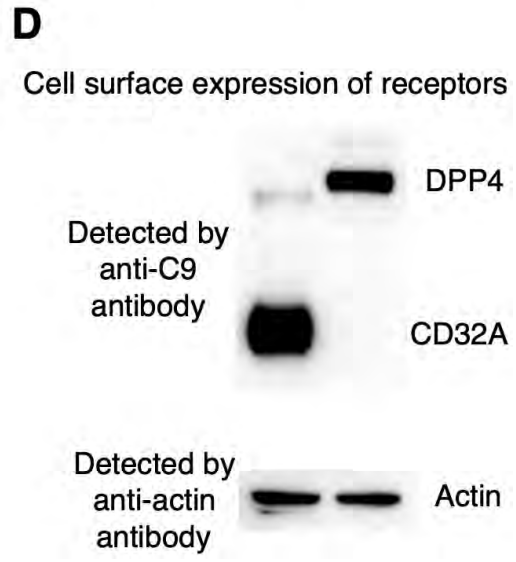
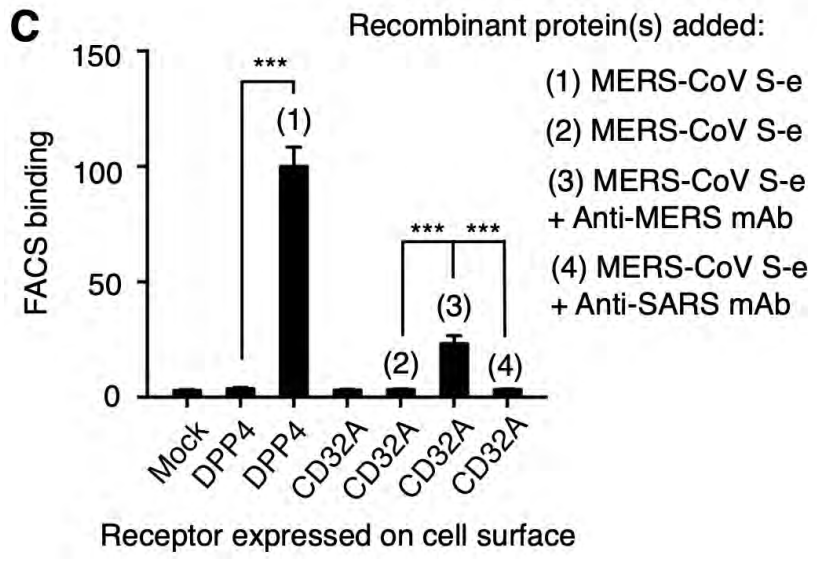
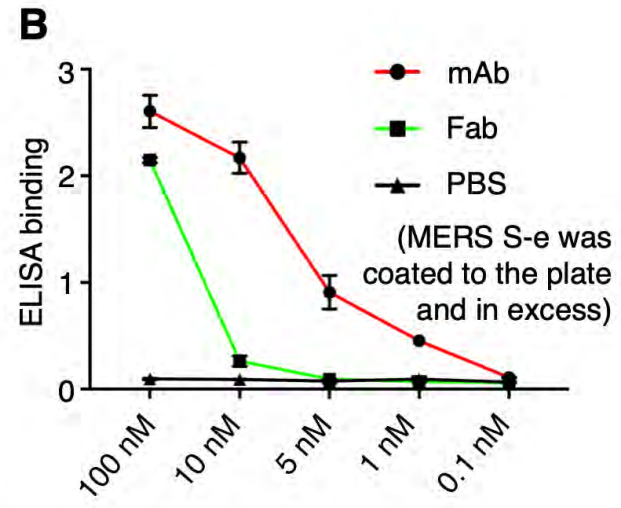
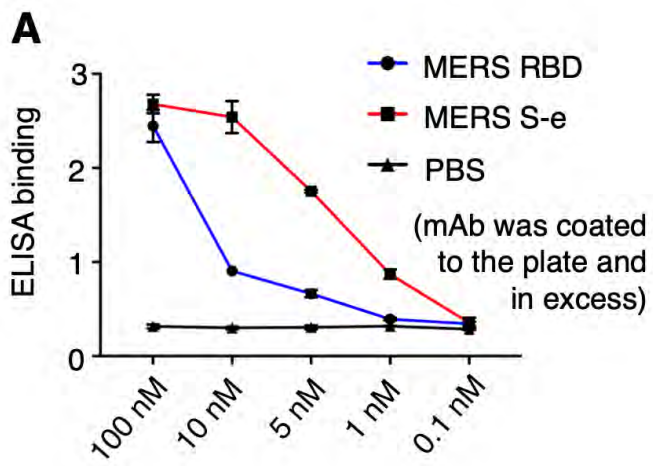
888 antibody binds to the side of the RBD, away from the viral-receptor-binding site,

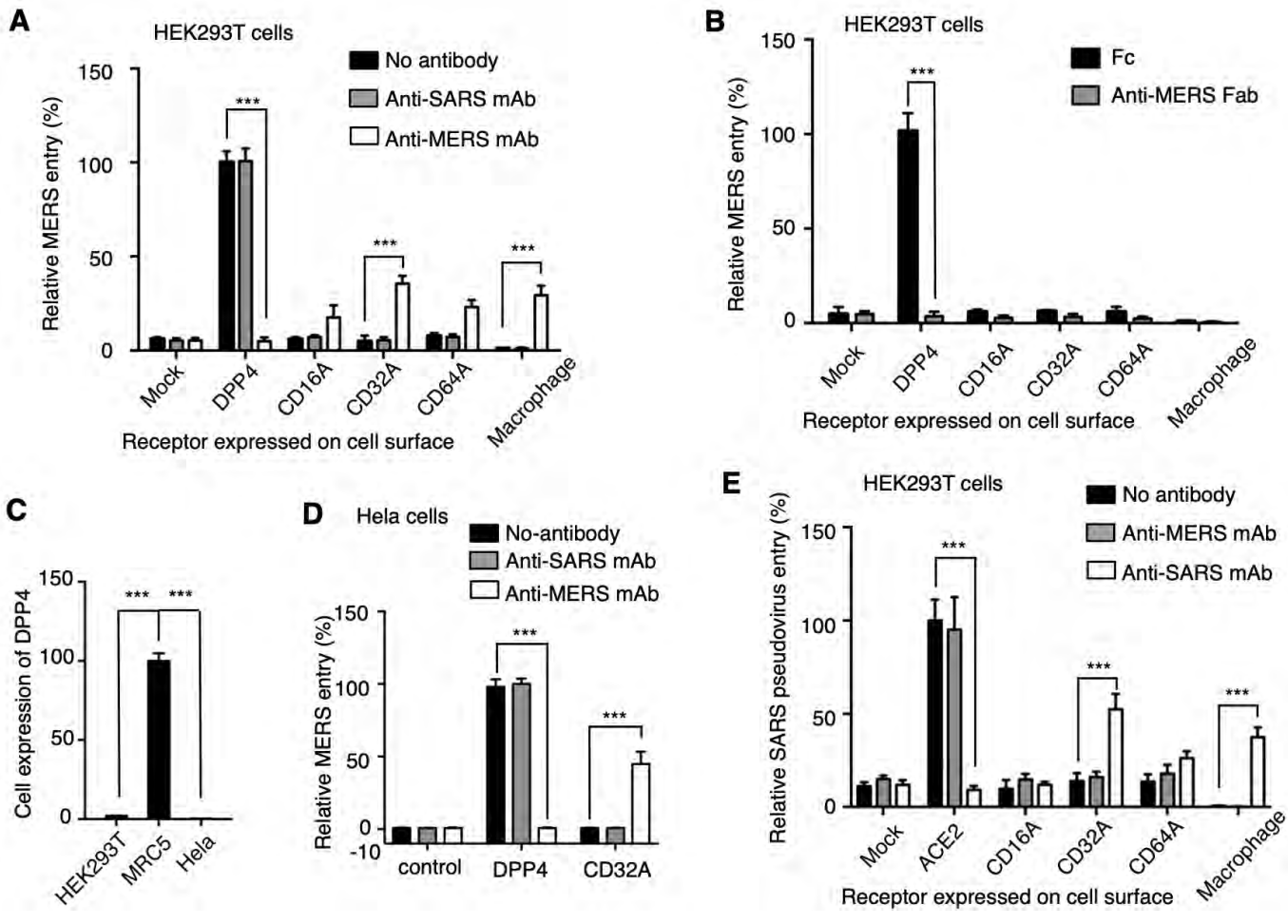
889 stabilizes the RBD in the lying-down state, and hence does not trigger conformational

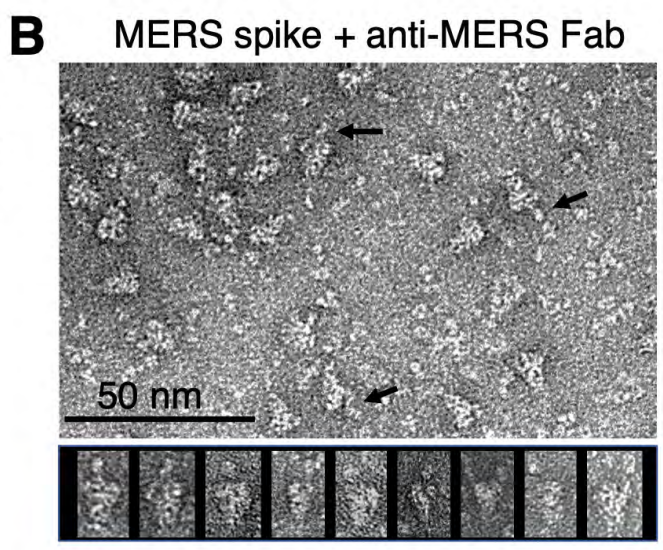
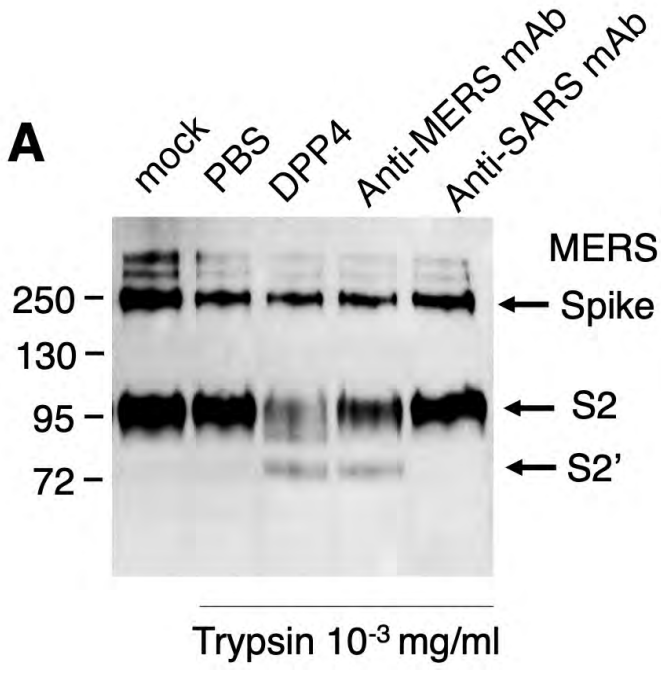
890 changes of SARS-CoV S-e. (B) MERS-CoV S-e complexed with LCA60 mAb (PDB ID:

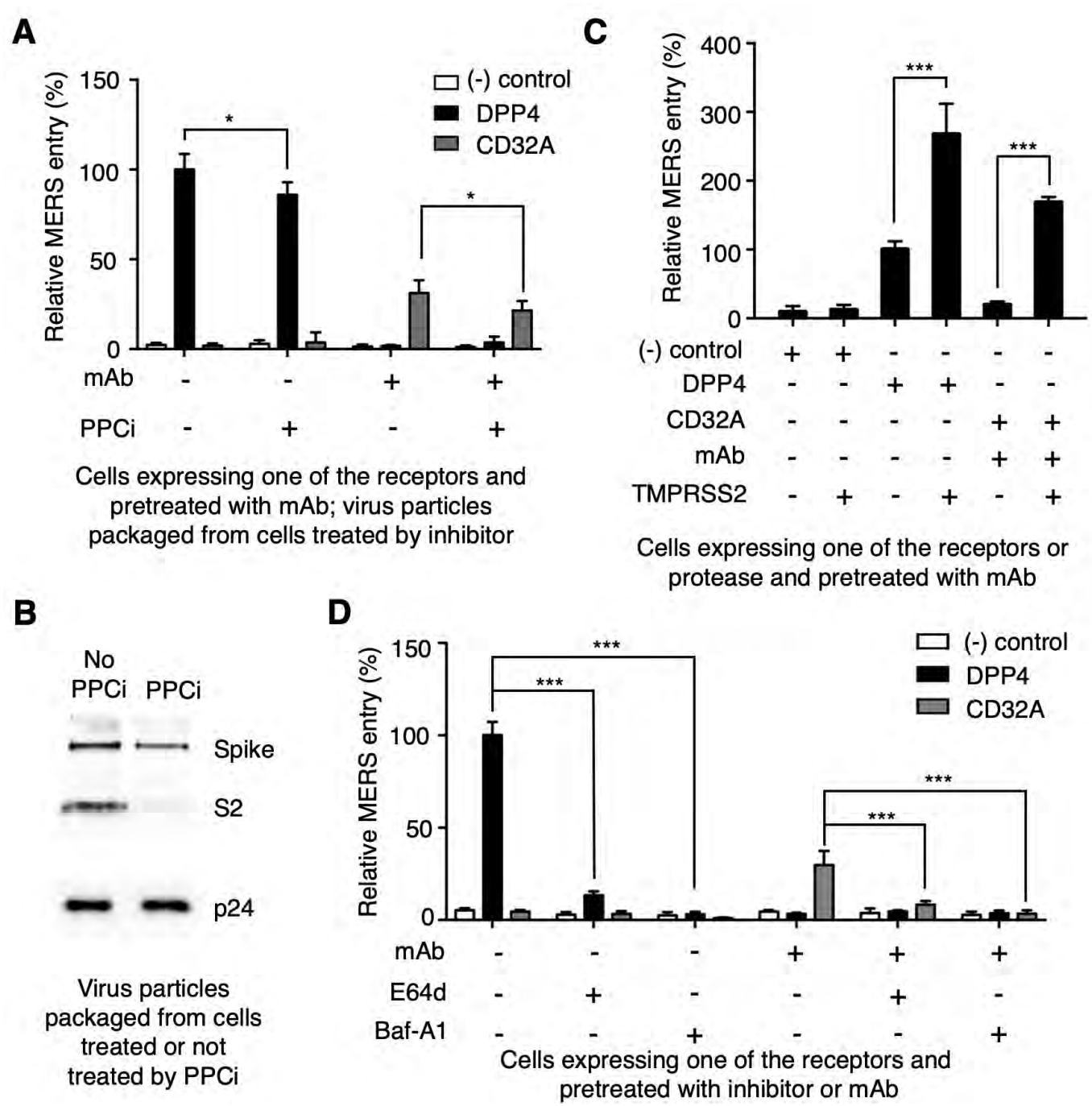
891 6NB4). The antibody binds to the viral-receptor-binding site in the RBD, stabilizes the
892 RBD in the standing-up state, and hence triggers conformational changes of MERS-CoV
893 S-e.

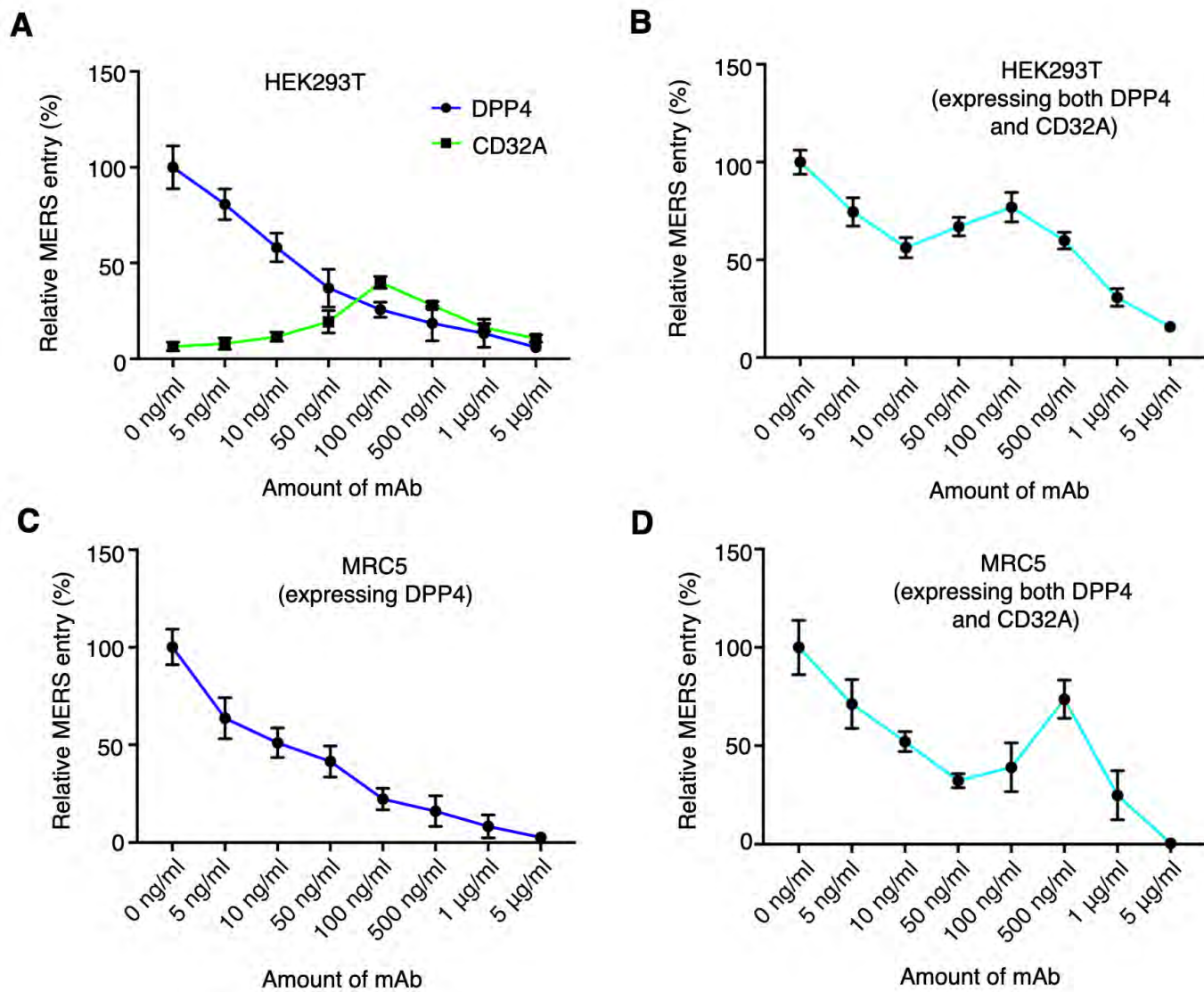




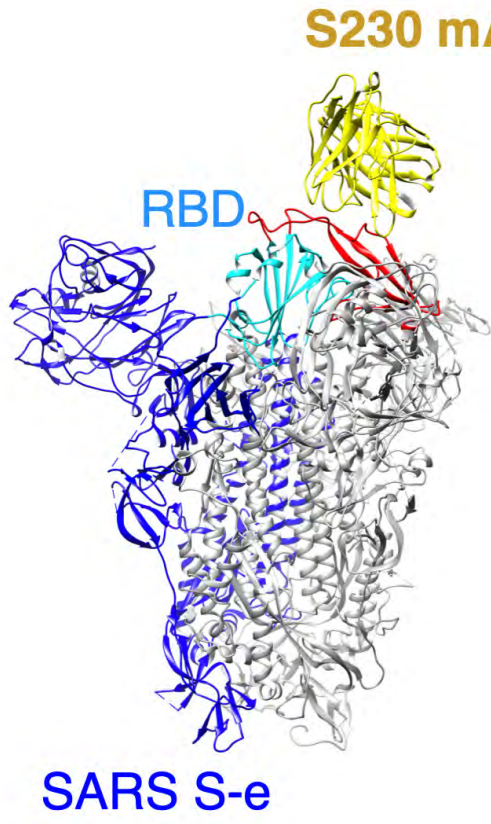








A



B

